STUDY OF HEAT TRANSFER FROM AN IMPINGING JET TO A SUBSTRATE

A Thesis by

Arjun Pokharel

B.S., Motilal Nehru Regional Engineering College, Allahabad, India, 1998

Submitted to the College of Engineering
and the Faculty of the Graduate School of
Wichita State University in partial fulfillment of the
requirements for the degree of
Master of Science

December 2005

STUDY OF HEAT TRANSFER FROM AN IMPINGING JET TO A SUBSTRATE

I have examined the final copy of this thesis for form and content and recommend that it be accepted in partial fulfillment of the requirements for the degree of Master of Science with a major in Mechanical Engineering.

_____

Ikrammuddin Ahmed, Committee Chair

We have read this thesis
and recommend its acceptance:

_____

T. S. Ravigururajan

_____

Krishna Krishnan

DEDICATION

To my parents Ambika Prasad Upadhyay and Sushma Upadhyay,

and wife Roshana Pokharel

ACKNOWLEDGEMENTS

First and foremost, I express my deep gratitude to Dr. Ikram Ahmed, who guided me as an advisor as well as research mentor during my efforts on this thesis. He was encouraging and very instrumental in the achievement of the goals of this work. He has had a tremendous impact on this thesis, and I have had immense pleasure working with him during my tenure at Wichita State University. Ms. Kristie Bixby deserves my humble gratitude for correcting my thesis multiple times.

I would also like to thank Dr. T. S. Ravigururajan and Dr. Krishna Krishnan for giving me important suggestions and comments for this project, and also serving on my thesis committee. My gratitude also goes to members of the Thermal/Fluid Science (TFS) research group for participating in open discussions and providing comments, and to the Wichita State University Department of Mechanical Engineering for providing me with an assistantship. I cannot thank enough the sincere and thoughtful efforts of Mr. Ildar Sabirov, my colleague and friend, who has helped me at every step of the process.

My parents deserve my deepest gratitude for standing by me and energizing me during the hardest of times. As my guardians and mentors, they are responsible for all the good things I have achieved in my life. My elder brothers, my source of inspiration, Dr. Anupam Pokharel and Dr. Arbinda Pokharel have always influenced me to move ahead.

Last but not least, the greatest thanks to my beloved wife, Roshana, who has always provided me with strength to move on, and who has stood by me throughout all my efforts.

ABSTRACT

A high-temperature argon-hydrogen plasma jet issuing into ambient air and impinging on a flat circular steel substrate was modeled using a commercial CFD software. Plasma was represented as an ideal gas with temperature-dependent thermodynamic and transport properties. The flow was governed by steady-state compressible Navier-Stokes equations with axisymmetry. Turbulence was modeled using the k-ε model. Chemical reactions and electromagnetic fields were not considered in this study. Two different cases were carried out: adiabatic and isothermal substrates. The recovery temperature and Nusselt number along the radial distance on the substrate were obtained for various Reynolds numbers. It is seen that radiation and air entrainment are equally important phenomena affecting the temperature distribution in a plasma jet issuing into ambient air and the subsequent heat transfer to the substrate.

TABLE OF CONTENTS

LIST OF FIGURES

CHAPTER 1

INTRODUCTION

Many applications in industry require localized heating or cooling, such as drying of paper and textiles, tempering glass, manufacturing bearings and turbine blades, and cooling electronics. An effective way to accomplish these processes is through the use of impinging gas jets. Impinging jets have been of much interest because they are widely used to produce high heat and mass transfer rates.

A special case of jet impingement heat transfer occurs during the plasma spray coating process. Plasma spraying is a process by which metallic or non-metallic particles are sprayed with a high-speed plasma jet on a substrate to be coated. Plasma coatings are widely used for surface modification in the manufacturing process. A detailed review of thermal spray technology is available in the monograph by Pawlowski [1] and the review article by Fauchais [2]. These coatings provide a strong resistance to wear, corrosion or high temperature, and can be used on metallic or non-metallic substrates.

The coating's adhesion and durability are the main focus in all plasma spray studies. Coating adhesion depends primarily on substrate preparation, preheating temperature, and the morphology and composition of the precursors used for coating deposition. Preheating of the substrate, generally achieved with a plasma spray jet without the coating precursor, is a key issue, and it must be controlled according to the size and thickness of the part to be sprayed. Substrate and coating temperatures during spraying are also linked to the coating's residual stress distribution, and therefore, it is very important to control this parameter. The degree of preheating

depends on spray torch geometry, plasma-forming gases, cooling systems, and torch – substrate stand-off distance.

The plasma jet parameters, such as temperature, thermal conductivity, specific heat, density and viscosity, depends on torch geometry, gas composition, flow rates, and arc power, which are key factors in governing the quality of coating. A reliable study of these parameters will provide a background for better control of the plasma jet.

The composition and properties of the enveloping atmosphere are equally important in entrainment in the plasma jet. The transport phenomena during coating deposition as well as the quality of final coating are likely to be different in different ambient conditions. Entrainment tends to degrade performance of the splat impingement process. Hence, understanding this process is critical.

The physical and chemical characteristics of the substrate as well as its distance from the plasma torch exit may also impact its preheating as well as the final quality of the coating.

Plasma is a very hot (10,000 to 18,000 K), ionized, gaseous state of matter. The plasma in a free jet undergoes a wide range of temperatures, decreasing sharply from the jet nozzle to the substrate. Due to the high temperature near the exit, particles injected into the jet melt before reaching the surface of the substrate. These partially or fully melted coating materials are carried toward the substrate surface where they solidify and build up a solid coating. Heat transfer from hot gases to solid surfaces occurs through both convection and radiation.

Although the jet temperature decreases considerably due to entrainment of the ambient gases in the plasma issuing from a jet, it is still high enough to melt a substrate if exposed for a long enough period of time, which is not desirable. On the other hand, limited preheating of the substrate can improve the quality of coating since the cold surface of a substrate can cause poor adhesion. The quality of the coating also depends on other parameters of the process, such as power input, gas flow rate, powder size, injection angle, surface roughness, substrate temperature, stand off distance, and the ambient atmosphere [3].

Plasma sprays can be experimentally studied in a spray booth, but this can be costly and time consuming. Computational Fluid Dynamics (CFD) has become more popular these days in modeling and analyzing plasma spray processes, not only because it is economic and efficient but also because the predicted results are continuously improving and are usually in close agreement with the experimental results.

A large number of studies have been done to investigate the heat and mass transfer from an impinging air or water jet to a substrate through numerical calculations and experiments [4-7]. These studies focused on the effect of stand-off distance, Reynolds number, free-stream turbulence, and nozzle-exit geometry orientation. However, few efforts have been made to calculate heat transfer from plasma to the substrate [3, 8] and to estimate heat flux and convection heat transfer coefficient, despite the great practical significance.

Obtaining the plasma temperature and convection heat transfer coefficient distribution along a substrate, as well as Nusselt number, during spraying is very

critical because these parameters are used as input data to calculate conduction within the substrate to estimate substrate preheating time. It is advantageous to optimize the distance between the plasma gun exit and the place of the particle injection into the jet to obtain the desirable level of particles melting to achieve the high-quality coating.

This study is parallel to the work by Sabirov [9], who is trying to estimate the heat flux from plasma to a substrate using inverse calculations.

Figure 1 shows the schematic representation of plasma spray coating deposition system. This study focused on calculating the heat flux from plasma jet to a substrate and recovery temperature of the plasma jet impinging on a flat circular substrate.

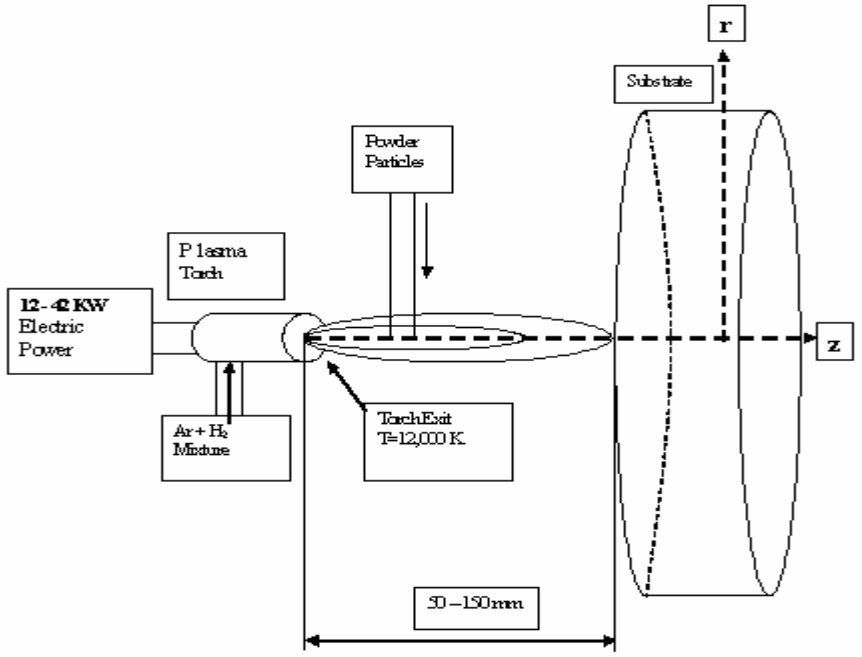

Figure 1. Schematic representation of typical plasma spray coating deposition system

CHAPTER 2

LITERATURE REVIEW

Thermal plasma technology has evolved into an advanced interdisciplinary science and is attracting increasing attention [1]. This technology is a highly complex process with many variables, as many as 50 to 60 spray parameters affecting the final splat formation parameters [2].

Liu et al. [3] modeled the flow-field of the plasma jet and correlated it with the process parameters such as total input power, plasma volume flow rate, and hydrogen contents in the Ar-H_2 mixture. They calculated the plasma jet temperature at the nozzle exit as well as axial temperature and velocity distributions for different input power, flow rate, and radial distance. Ogawa and Hijikata [8] have analyzed the effect of joule heating, re-combination of charged particles and electron working function on the heat transfer between the plasma jet and a wall. Baughn and Shimizu [10], Lee et al. [11], and Yan et al. [12] have modeled local transfer coefficients for a fully developed axisymmetric air jets impinging on a flat surface. They used the steady-state model to calculate the heat transfer parameters. Yan et al. [12] has also shown that Reynolds number is one of the most important parameters affecting the heat transfer in plasma spray. The works of Martin [4], Goldstein and Timmer [13], and Obot et al. [14] have resulted in the establishment of empirical correlations for evaluating local or area mean heat transfer for air jet. Obot et al. [14] have shown that the nozzle exit configuration is the most important factor that affects heat transfer near the stagnation point. Gordon and Akfirat [15] have studied the effects of turbulence on heat transfer from impinging two dimensional and circular jets in the

zone around the stagnation point. They showed that for small nozzle to plate distances for circular jets, the Nusselt number may show a relative minimum for the stagnation point in a plot showing the lateral variation of Nusselt number.

Baukal and Gebhart [16] studied flame impingement, related temperature with radial distance and the centerline temperature with axial distance for three steady-state cases: uncooled target, cooled target and cooled heat flux gage. They have shown the graphs of temperature and velocity along the axial distance. Boguslawski and Popiel [17] performed measurements of radial and axial distributions of mean velocity, kinetic energy, turbulent intensities and radial distributions of the turbulent shear stress in the initial region of a turbulent air jet issuing from a long round pipe into atmosphere. They found that the highest turbulence occurs at an axial distance of about 6d and radius of 0.7 to 0.8 d.

Hollworth and Wilson [18] and Hollworth and Gero [19] studied how distributions of the recovery factor and the effectiveness depend on the spacing from the jet exit to the impingement place. Hoogendoorn [20] studied the effects of turbulence on heat transfer at the stagnation point of impinging jets, and data on the variation of local heat transfer coefficient produced by impinging jets were re-examined. For smaller nozzle to plate distances it was shown that Nusselt number at the stagnation point is smaller than for points in the region directly around it.

Lytle and Webb [21] measured the local heat transfer rate and flow structure at a nozzle-to-plate spacing less than one nozzle diameter and found the existence of inner and outer peak in the local heat transfer near the stagnation point. Kataoka [22]

investigated the role of artificially induced large-scale eddies on the impinging heat transfer.

In experimental studies of jet-impingement heat transfer, researchers have used different temperature measurement devices such as thermocouples and IR-cameras to measure the temperature of the impinged surface [5,18,19], but in the present study, an axisymmetric 2D model based on the finite volume method was used for modeling the heat transfer from a plasma jet to a steel substrate. A commercial CFD software was used to estimate the plasma temperature and heat flux at the impinged (substrate) surface. Values of density, enthalpy, specific heat, viscosity, thermal conductivity, and electrical conductivity as a function of temperature (for a range of temperatures from 500 to 15,000 K), published by Boulos et al. [23] for argon, hydrogen, and air were used in this study. Experimental data were used as references in order to verify some of the results. A grid independence study was also performed.

CHAPTER 3

METHODOLOGY

3.1 Problem Description

Inside a plasma torch nozzle, a DC discharge occurs between a copper anode and a tungsten cathode, to which the electrical power in the range of 5 to 200 kW is supplied. The gas to be ionized passes through the cylindrical space that extends between the cathode tip and the axis of the exit nozzle of the torch. The electric current enters this space from the cathode tip and exits at the other end of the arc column through the gas that forms an electric bridge. Most of the electric energy in the plasma torch is converted to heat and ionization. Water is circulated externally around the plasma torch for preventing the hardware from melting.

In this study, the formation of plasma inside the torch was not modeled. The plasma is modeled as a single species consisting of 80% Ar and 20%. The primary gas, argon, has a high density and a relatively low thermal conductivity (k = 1.5 W/m.K at 12,000 K), while the secondary gas, hydrogen, has a low density and a higher thermal conductivity (k = 5.4 W/m K at 12,000 K) [3]. The plasma jet issues into the quiescent atmosphere through an 8 mm orifice. The surrounding air was assumed to have a temperature of 300 K. The plasma, assumed to be axisymmetric, impinged on a flat circular substrate, assumed to be a flat surface, 0.05 m from the nozzle. A commercially available CFD code was used to predict the temperature and heat flux at the substrate. Since plasma emits significant radiation above temperatures of 5,000 K [23], gas phase radiation was included in the final calculations for this study.

3.2 Assumptions

The gaseous species behave as ideal gases at atmospheric pressure. The system is steady, with time-averaged turbulent fluctuations taken into account. Plasma components and the flow of plasma are in local thermodynamic equilibrium (LTE). LTE is a condition under which matter emits radiation based on its intrinsic properties and its temperature, uninfluenced by the magnitude of any incident radiation [25]. LTE occurs when the radiant energy absorbed by a molecule is distributed across other molecules by collisions before it is reradiated by emission. The electric discharge is in steady-state with constant power value, and electric and magnetic forces are disregarded. The gravity force is negligible compared to the kinetic effects. No ionization or chemical reaction takes place.

3.3 Governing Equations

The equations solved for the plasma-air interaction were conservation of mass, momentum, enthalpy, radiative energy, species (argon, hydrogen, and air), turbulence kinetic energy, and dissipation.

Conservation of Mass: The continuity equation is the reflection of the continuum medium assumption. The physical meaning of this equation is that the fluid will occupy continuously every point of space in the flow domain. As applied to a system, this principle states that mass of a fluid remains constant. As applied to a control volume it states that as flow passes through a fixed volume in space, if the rate at which mass flows out of the volume is greater that that entering the volume, there must be a corresponding decrease in mass inside the volume. Furthermore, if the

fluid is incompressible, so that the mass per unit volume cannot change; the mass rate in must equal to mass rate out. More simply, under these circumstances the volume rate of flow in must equal the volume rate of flow out.

$$\vec{\nabla}.(\rho \mathbf{V}) = 0 \tag{1}$$

Momentum Equation: The momentum equation relates the acceleration of a fluid element to the forces acting on it in accordance with Newton's second law of motion. These forces include surface forces as well as body forces. However, body forces are assumed negligible in this study.

$$\vec{\nabla}.(\rho \mathbf{V}\mathbf{V}) = -\vec{\nabla}(p) + \vec{\nabla}.(\tau_{eff}) \tag{2}$$

In equation (3), τ_{eff} is the stress tensor with the molecular viscosity replaced by effective viscosity μ_{eff}, where

$$\mu_{eff} = \mu + \mu_t \tag{3}$$

The turbulent viscosity μ_t is determined through the RNG (renormalization group) extension of *k-ε* turbulence model. RNG *k*-ε is more accurate than the standard *k-ε* model because it has an additional term in its ε equation [26].

Enthalpy Equation: The fluid enthalpy, h, is defined as

$$h = \int_0^T C_{pg}\, dT \tag{4}$$

where C_{pg} is the specific heat of the plasma air mixture, and T is the absolute temperature of the fluid.

Density, ρ, is a function of pressure "p" and temperature "T" and can be defined from the ideal gas law:

$$\rho = \frac{pM}{RT} \quad (5),$$

where M is molecular weight of a fluid, and R is the universal gas constant.

The temperature of the plasma jet can be obtained once the enthalpy is known, hence the reason for an enthalpy equation. The reason for choosing enthalpy rather than temperature as a variable is that the specific heat of the plasma is a function of temperature, and temperature does not satisfy the energy conservation law while enthalpy does. The transport equation for the fluid enthalpy is written as

$$\vec{\nabla}.(\rho h V) = \vec{\nabla}.k_{eff}\vec{\nabla}(T) - \vec{\nabla}.\mathbf{q}_r \quad (6)$$

where k_{eff} is the thermal conductivity, and $\mathbf{q}_r$ is the source term that represents the heat energy lost from a given volume due to radiation. The determination of this has been explained by Modest [25].

$$-\mathbf{q}_r = -4\int \acute{\alpha}_\lambda e_{\lambda b}(\lambda,T)d\lambda + \int\int \acute{\alpha}_\lambda i_\lambda(\lambda,\omega)d\omega d\lambda \quad (7)$$

The radiative flux is determined by balancing the local emission and local absorption of thermal radiation. Here, $e_{\lambda b}$ is the spectral blackbody emissive power, i_λ is the spectral radiative intensity, and $\acute{\alpha}_\lambda$ is the spectral absorptivity of the gases. The radiative transfer is modeled with the P1 approximation for diffuse radiation, yielding

$$-\mathbf{q}_r = -4\kappa\sigma T^4 + \kappa G \quad (8)$$

where $\kappa = \kappa(T)$ is the Plank's mean absorption coefficient [23], and G is the incident radiation.

Species Equation: The mixing of the two species considered here plasma and air is determined by

$$\vec{\nabla}.(\rho m_i \mathbf{V}) = \vec{\nabla}.(\rho D_{eff}\vec{\nabla}(m_i)) \quad (9)$$

where the subscript "i" refers to the mass of the i^{th} species, and D_{eff} is the effective diffusive coefficient of Ar-H_2 in air.

The *k-ε* Two-Equation Turbulence Model: Using the *k-ε* turbulence model, the only additional independent variables introduced are the turbulence energy *k* and its dissipation rate *ε*. The turbulence stress tensors are linked with the Reynolds averaged flow velocity component using

$$\tau_t = (2\ \mu_t \mathbf{S} - \frac{2}{3}\rho k \mathbf{I})\ \nabla \mathbf{V} \tag{10}$$

where τ_t is the Reynolds stress, **S** is the symmetric part of the velocity gradient, **I** is the identity matrix, *k* is the turbulence kinetic energy of unit mass defined by

$$k = \frac{1}{2}(\overline{u'}^2 + \overline{v'}^2 + \overline{w'}^2) \tag{11}$$

and μ_t is the turbulence viscosity, which can be determined by the turbulence models. These relationships provide the six equations for the six Reynolds stress variables. However, they introduce one additional variable, viscosity μ_t. In the present study, the *k-ε* turbulence model is applied, and this model links the μ_t with the turbulence energy *k* and its dissipation rate *ε* as

$$\mu_t = C_\mu \rho_g \frac{k^2}{\varepsilon} \tag{12}$$

where C_μ is a model constant, and *k* and *ε* are determined by the transport equations

$$\nabla.(\rho k \mathbf{V}) = \nabla.((\alpha_k \mu_{eff})\nabla(k) + \mu_t S^2 - \rho\varepsilon \tag{13}$$

$$\nabla.(\rho \varepsilon \mathbf{V}) = \nabla.((\alpha_\varepsilon \mu_{eff})\nabla(\varepsilon)) + C_{1\varepsilon}\mu_t S^2 \frac{\varepsilon}{k} - C_{2\varepsilon}\rho\frac{\varepsilon^2}{k} - R \tag{14}$$

The turbulent viscosity μ_t, the inverse Prandtl numbers α_κ and α_ε, the effective thermal conductivity and species diffusivity, and the quantities C_μ and R are determined through the RNG extension of the *k-ε* turbulence model [24]. $C_{1\varepsilon}$ and $C_{2\varepsilon}$ have the values of 1.42 and 1.68, respectively. S is the strain tensor, in Cartesian coordinates,

$$S_{ij} = \partial_{(i} v_{j)} = \frac{1}{2}\left(\frac{\partial v_j}{\partial x_i} + \frac{\partial v_i}{\partial x_j} \right)$$

In other words, S is the symmetric part of the velocity gradient, $\overset{\mu}{\nabla}\mathbf{V} = \partial_i v_j$

The effective transport properties are dominated by the turbulent quantities.

3.4 Boundary Conditions

The boundary conditions were based on the physical configuration of the computational domain shown in Figure 2. Two different cases were considered in the present study: adiabatic and isothermal substrates. Both cases were again considered with and without radiation to see the impact of radiation on plasma temperature as plasma impinged on the substrate.

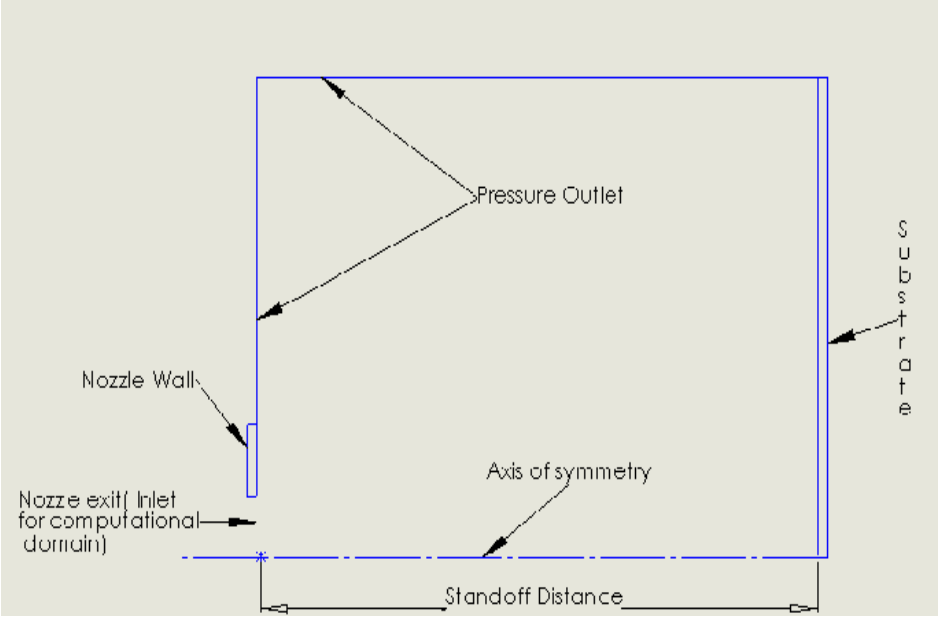

Figure 2. Computational domain for modeling plasma issuing into ambient air (nozzle exit radius 4 mm, nozzle wall thickness 8 mm, substrate radius 50 mm, stand-off distance 50 mm).

Figure 2 represents the axisymmetric computational domain considered in this study. A nozzle with an orifice diameter of 8 mm surrounded by a 4 mm-thick wall issued the plasma which fully develops into 12,000 K into a quiescent ambience normally toward the flat round substrate wall. The plasma torch exit temperature, 12000K does not depend upon the Reynolds number but it does depend upon the plasma power input. The substrate had a 50 mm radius and was located coaxially at a standoff distance of 50 mm from the nozzle. The initial temperature of the wall was assumed to be 300 K, which is normal room temperature. The influence of the DC arc fluctuations, which are originally driven by random arc initiation and extinction between cathode and anode, is not a true turbulence phenomenon. However, because of the lack of understanding of the detailed arc physics, the fluctuation was accounted for by specifying a high level of turbulence at the jet exit, with the turbulence intensity to be 20 percent [24]. The plasma jet velocity at the inlet of computational

domain was varied from 200 m/s to 1,040 m/s. The radiation heat loss was solved by using the P1 approximation for diffuse radiation. The simulation was initialized by filling the computational domain with quiescent ambient cold air, which was then displaced by, and mixed with, the incoming argon plasma until steady-state was reached. The final steady solution was assumed to be unique and independent of the initial conditions and transient history.

The substrate was considered a solid surface since this problem focused on obtaining the recovery temperature and heat flux distribution along the radial distance on the substrate impinged surface. Two cases have been considered: adiabatic substrate and isothermal substrate. No-slip boundary conditions were assumed for the substrate. Heat conduction within the substrate was a parallel problem, as studied by Sabirov [9].

3.5 Computational Method

The finite volume code FLUENT was used to solve the above set of equations to achieve the results of this study. The assumptions used here were: steady state, axisymmetric computational domain, and explicit scheme.

The governing equations have been discretized using the first order upwind scheme, except for the pressure and pressure-velocity coupling (SIMPLE scheme). The second order upwind scheme is recommended for triangular and tetrahedral grids [26]. For simple square grid the first order discretization provides low numerical discretization error (numerical diffusion). In addition, first order discretization provides better convergence than second order discretization. The convergence criteria was user-prescribed and equal to 10^{-6}.

CHAPTER 4

RESULTS

4.1 Grid Independence Study

In the present study, a number of different grid sizes for the finite volume method code were considered in order to check the sufficiency of the mesh resolution. Three different uniform mesh sizes, measured by the number of grid points, were finally compared: 80 x 50 (80 axial and 50 radial), 160 x 100 and 320 x 200. The mesh was more refined near the axis (in the radial direction) as well as near the jet (in the axial direction). An estimate of error was made by comparing coarse grid solutions against those from the finest grid.

$$error = \frac{|\Delta T_{coarse} - \Delta T_{fine-mesh}|}{\Delta T_{fine-mesh}} \tag{15}$$

where, ΔT is the difference in stagnation point and ambient temperatures. From the calculations, the error between the coarsest and intermediate meshes was 8.7% and that between the intermediate and fine meshes was 3.2% (see Figure 3).

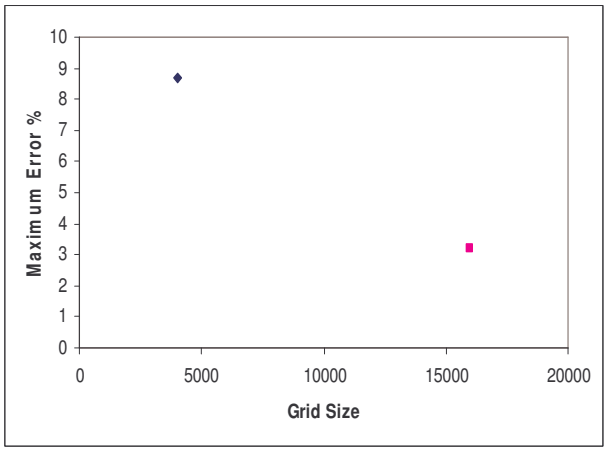

Figure 3. Error calculation for different grid sizes.

4.2 Observations

The solutions for temperature, air mass fraction, and heat fluxes were observed. Figure 4 presents the temperature field for the both cases. Comparison between the temperature with and without radiation in is shown in Figure 5. It has also been found that when radiation is taken into account the temperature throughout the computational domain is relatively lower. The experimental data and the computational data are also relatively closer. It is seen that temperature decrease sharply in the experimental process than in the computational process. This is seen near the plasma torch exit for about 15 mm, but after about 15 mm the obtained results in this result and the experimental result follow the similar curve pattern upto the stagnation point of the substrate. Similarly, the radial temperature distribution at the substrate is shown in Figure 6.

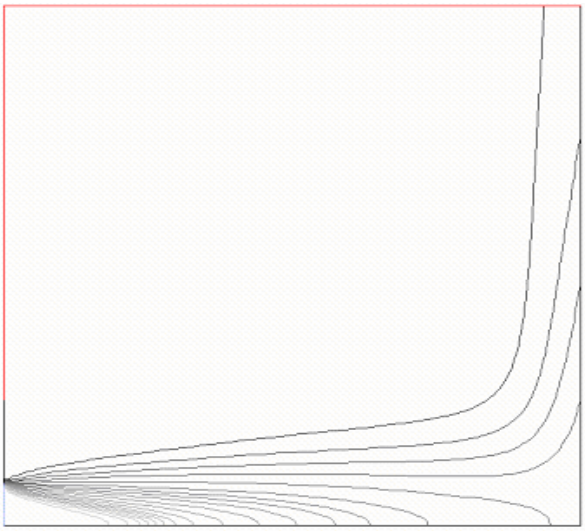

Figure 4. Temperature contour in the computational domain.

(Maximum temperature 12000K, Minimum temp 300K, Increment temperature 580K)

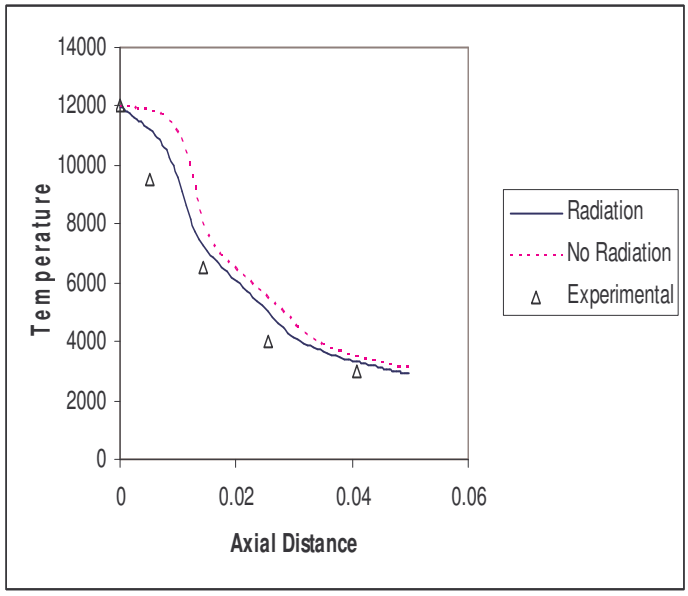

Figure 5. Temperature distribution along the jet axis.

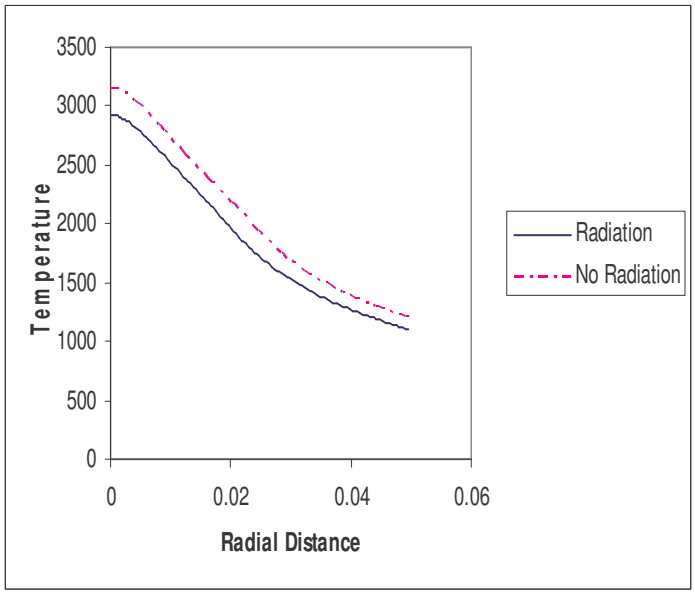

Figure 6. Temperature distribution along substrate radial direction.

Observation of the air mass fraction contour is shown in Figure 7. Mass fraction of air is plotted against the jet axis in Figure 8, and against the substrate

radial distance in Figure 9. Entrainment is shown in terms of percentage, and it can be seen that entrainment of air in the plasma near the jet exit is $< 5 \times 10^{-5}$ %, i.e., there is almost no entrainment near the jet exit. This shows that the temperature decline of plasma from the nozzle exit was due to radiation only, further increased by air entrainment when it becomes significant at about 6 mm from the nozzle exit. Entrainment increases to almost 90% at the farthest radial corner of the substrate and is almost the same in both the radiation and no-radiation conditions, which is shown in Figures 8 and 9.

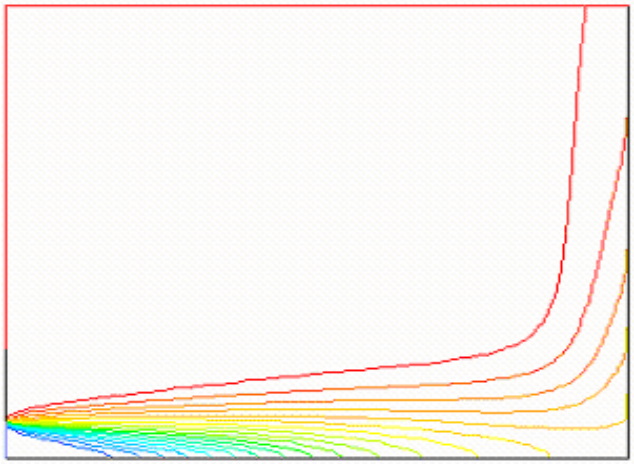

Figure 7. Contour of mass fraction of air inside the computation domain. (Maximum air fraction 100%, Minimum Air fraction: 4 X 10^{-17}%, Increment 5%)

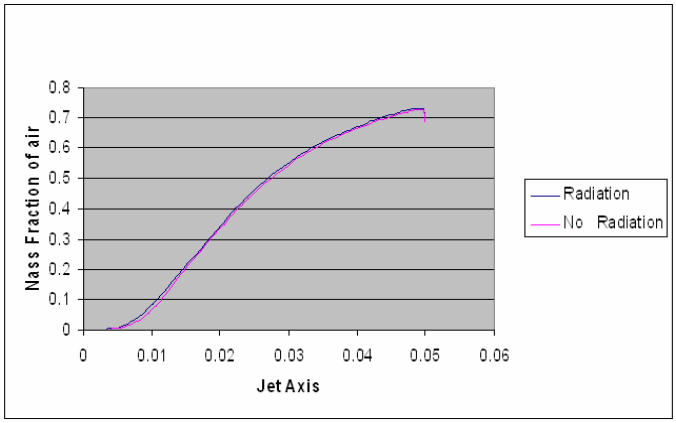

Figure 8. Mass fraction of air along the jet axis.

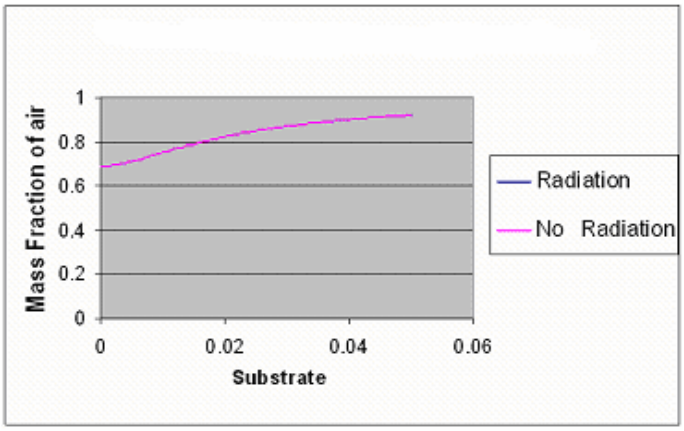

Figure 9. Mass fraction of air along the substrate.

4.3 Calculations

In order to estimate the substrate heating, i.e., for the conduction of heat into the substrate, the heat flux distribution along the substrate needs to be predicted. Alternatively one can calculate the heat flux if the temperature distribution as well as the transfer coefficient distribution is known. In the absence of any standard thermal boundary conditions on the back side of the substrate, two extreme cases were studied: adiabatic substrate with its back and edge insulated, and an isothermal

substrate with its temperature held at 300K. In the first case, the substrate reaches what is referred as the recovery temperature for the plasma. In the second case, heat flux from the plasma to the substrate is calculated. The two sets of results were used for an estimation of the local heat transfer coefficient, h.

Torch exit conditions were characterized by the Reynolds number. In the plasma jet, the Reynolds number is defined as

$$\mathrm{Re} = \frac{\rho_g U_o d}{\mu_g} \tag{16}$$

The recovery temperature obtained on the adiabatic substrate is represented as a non-dimensionalized temperature (NDT):

$$NDT = \frac{T_{recovery} - T_{subs}}{T_{jet} - T_{subs}} \tag{17}$$

this is later scaled by the stagnation point temperature and expressed as the normalized non-dimensional temperature (NNDT):

$$NNDT = \frac{\dfrac{T_{recovery} - T_{subs}}{T_{jet} - T_{subs}}}{NDT_{stag}} \tag{18}$$

Local heat transfer was measured, with the following relations,

$$Nu = \frac{hd}{k} \tag{19}$$

$$h = \frac{q''}{\left(T_{recovery} - T_{subs}\right)} \tag{20}$$

where Nu = Nusselt number

d = nozzle diameter

k = thermal conductivity of plasma along the radial distance of the substrate

h = coefficient of convective heat transfer of plasma along the substrate radial distance

q" = heat flux of plasma along the radial distance of the isothermal substrate

$T_{recovery}$ = recovery temperature at the adiabatic substrate.

Using equation (16), it was determined that all of the flows considered in this study were turbulent, Re > = 4,000. The recovery temperature and local heat transfer along the radial distance in the substrate were calculated for each of the flows which are shown in Figures 10 to 14.

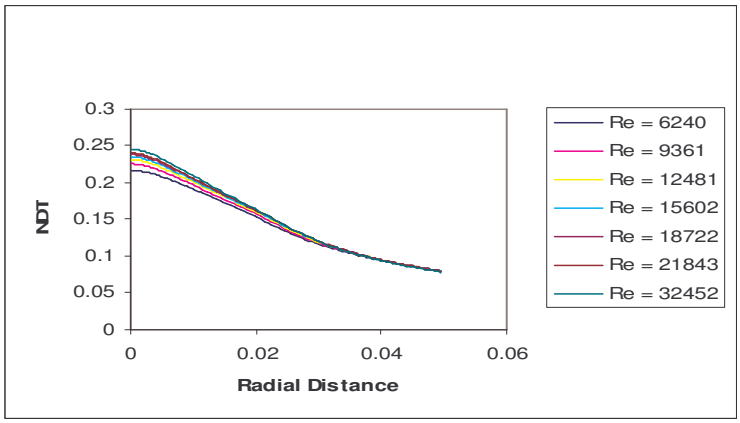

Figure 10. Distribution of non-dimensional temperature on the substrate (without radiation).

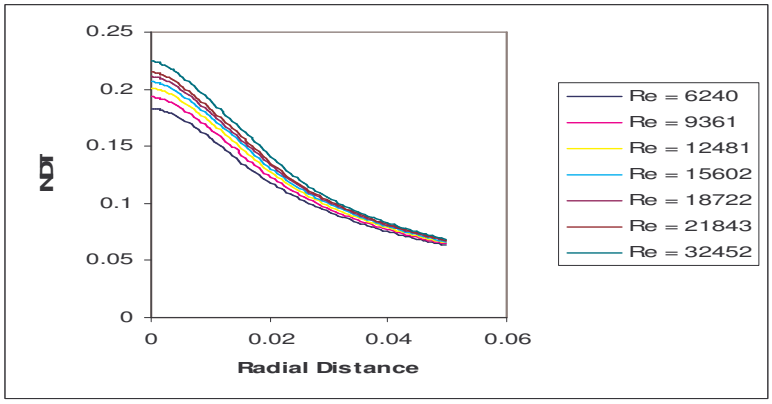

Figure 11. Distribution of non-dimensional temperature on the substrate (with radiation).

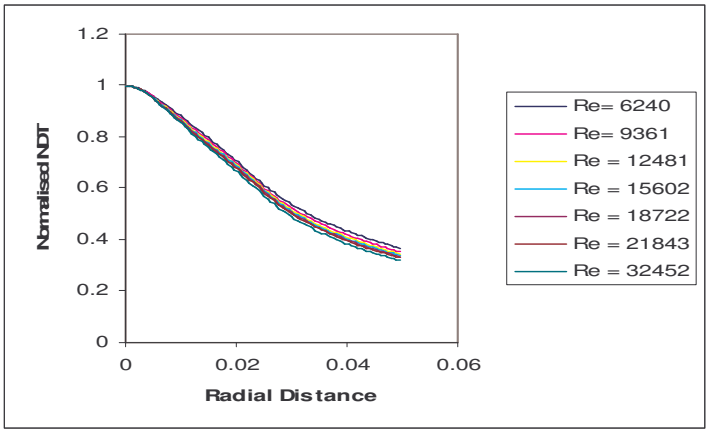

Figure 12. NNDT along the radial distance at substrate (without radiation).

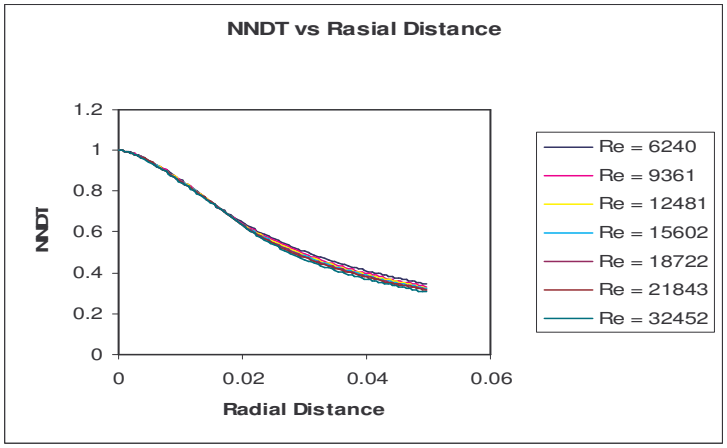

Figure 13. NNDT along the radial distance at substrate (with radiation).

Similarly, the Nusselt number along the radial distance in the substrate was calculated for each of the flows using equations (19) and (20) which are shown in Figure 14. Figures 14 and 15 were compared for similarity.

Martin [4] calculated Sherwood number and Lee et. al [5] calculated the nusselt number.

The Nusselt number calculation in this study was based on the principle used by Lee et al. [4]. They defined Nusselt number as,

$$\text{Nu} = \frac{hd}{k}$$

Where

h=convective heat transfer coefficient

d = diameter of torch exit

k = thermal conductivity of plasma

$$\text{h} = \frac{-q''}{T_{recovery} - T_{subs}}$$

The authors have calculated the heat flux q" using a heat-flux gauge made of thermopiles.

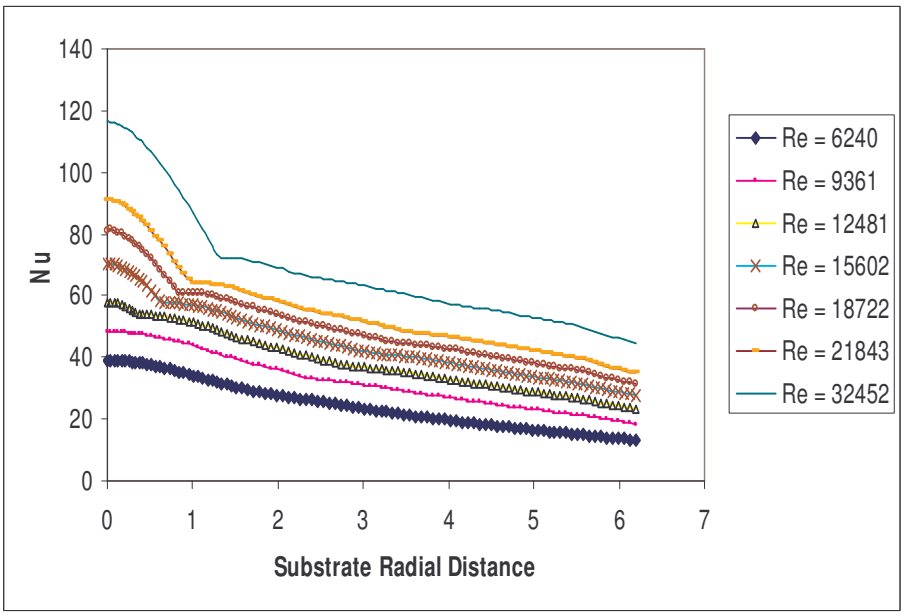

Figure14. Nusselt number along the substrate (with radiation).

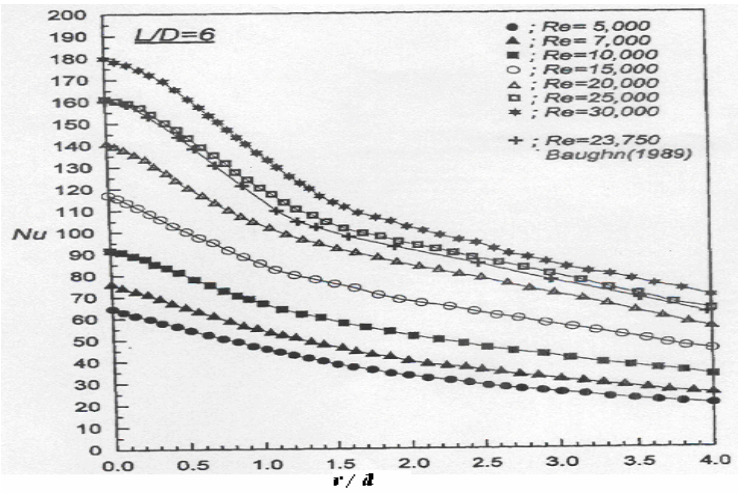

Figure15. Variation of the local Nusselt numbers [5].

4.4 Discussion

The plasma jet temperature decreased along the jet axis as it approached the substrate due to radiation, which also affected the plasma temperature distribution and local heat transfer along the substrate. The effect of radiation at the temperature and local heat flux distribution along the radial distance of the substrate was observed. The centerline temperature provided an idea of how radiation and air entrainment caused a drastic temperature decrease along the jet axis toward the substrate. That is why although the substrate is only 50 mm from the jet axis; the temperature of the plasma is considerably lower near the substrate than at the jet nozzle.

Figures 10 and 11 show the recovery temperature profiles obtained on the substrate in the radial direction in non-dimensionlized form. The non-dimensionalized temperatures were normalized to see if the data collapsed into a single curve, as shown in Figures 12 and 13

The Nusselt number was measured assuming the substrate wall to be isothermal. Figure 14 shows the distribution of heat flux into the isothermal substrate. The heat transfer along the radial distance on the substrate was expressed in terms of the Nusselt number, where heat flux q" was obtained from the CFD results. The Nusselt number calculation was done to study the distribution of local heat transfer.

As noted before, lower plasma temperatures were observed when radiation was taken into account. But, radiation affects heat loss up to the point where plasma reaches a temperature of about 5,000 K. After the plasma reached 5,000 K, it was only the air entrainment that reduced the temperature of the plasma. Since, the stagnation temperature was around 3,000 K, the temperature distribution and heat transfer along the substrate was not affected by radiation. Similarly, normalized NDT was plotted for models with and without radiation to see if the curves collapse into one. The normalized NDT almost collapsed into a single curve as the jet approached the stagnation point, for a temperature range of Reynolds numbers from 6,240 to 32,500. The recovery temperature was maximum at the stagnation point, decreased monotonically outward along the impingement plate, and did not show any secondary maxima.

Similarly, as shown in Figure 14, the Nusselt number was plotted against the substrate radial distance. The Nusselt number decreased gradually for a lower Reynolds number but became increasingly steeper near the stagnation region for a higher Reynolds number. A secondary maxima was not present at all. The maximum heat transfer rates occurred at the stagnation point. The Nusselt number, i.e., the non-dimensional heat transfer, tended, in general, to increase with an increasing Reynolds

number, although at a different rate. It is also shown that Nusselt number was low and relatively uniform for lower Reynolds number, but as the Reynolds number increased, the decrease in heat transfer was sharp near the stagnation region. The profile of Nusselt numbers calculated from CFD solutions were compared with the work done by Lee and Lee [5] and found to be similar.

CHAPTER 5

CONCLUSIONS

In this study, CFD simulation of heating a substrate by an impinging plasma jet was performed for a 2D axisymmetric steady-state case. The recovery temperature and local heat-transfer characteristics on the impinged surface of the substrate were investigated. This study was done for a range of Reynolds numbers ($6{,}000 < Re < 33{,}000$) for a fixed standoff distance and substrate diameter. The code was based on the finite volume method and was found to be grid-independent. The NDT, normalized NDT, and Nusselt number for adiabatic and isothermal conditions with and without radiation were reported. Significant conclusions are as follows:

a. The centerline temperature distribution shows that radiation is the major cause for rapid decrease of temperature of impinging jet near the nozzle issuing the plasma jet. Entrainment of air helps in decreasing the temperature after certain axial distance from the plasma nozzle. Hence, the effect of radiation must be taken into account, although its effect is mostly in reducing the temperature before it impinges the substrate.

b. Profiles of dimensionless recovery temperature were calculated on a flat circular adiabatic plate model normal to the jet axis. Temperature profiles were normalized to observe the self similarity. These curves were used to predict the variation of recovery temperature associated with the fully developed wall jet. The temperature was maximum at the stagnation point and decreased gradually.

c. Nusselt numbers were calculated along the radial distance of an isothermal substrate. As expected, heat transfer was higher near the stagnation point and dropped off with radial distance. There were no secondary maxima. Heat transfer along the substrate was relatively uniform for lower Reynolds numbers than for higher ones. Hence, intense localized heating or uniform heating would depend upon the choice of the Reynolds number. The profiles of temperature and Nusselt numbers were compared with other published results and found to be qualitatively similar.

CHAPTER 6

SUGGESTION FOR FUTURE WORK

a. The problem that has been solved in this work was for steady state. The plasma temperature distribution along the substrate was constant. In practice, due to the contact with a cold substrate, the plasma temperature initially decreases significantly. Consideration of transient case (unsteady state) is necessary for a better understanding of more practical application.

b. Based on CFD predictions, a simple empirical or graphical result may be developed for plasma jet impingement heating.

c. Inverse calculations with experimental data may be compared to further verify and benchmark our results.

REFERENCES

LIST OF REFERENCES

1. Pawlowski, L., 1995, *The Science of Engineering of Thermal Spray Coatings*, John Wiley & Sons, New York, Chapter 1.

2. Fauchais, P., 2004, "Understanding Plasma Spraying," *J. of Physics: Applied Physics*, pp. R86-R108.

3. Liu, B., Zhang, T., and Gwane, D. T., 2000, "Computational Analysis of the Influence of Process Parameters on the Flow Field of a Plasma Jet," *Surface and Coatings Technology,* **32**, pp. 202-216.

4. Martin, H., 1977, "Heat and Mass Transfer between Gas and Solid Surfaces," *Advances in Heat Transfer*, **13**, Academic Press, New York, pp. 1-60.

5. Lee, J., and Lee, S. J., 1999, "Stagnation Region Heat Transfer of a Turbulent Axisymmetric Jet Impingement," *Experimental Heat Transfer*, **12**, pp. 137-156.

6. Viskanta, R., 1993, "Heat Transfer to Impinging Isothermal Gas and Flame Jets," *Exp. Thermal Fluid Sci*., **6**, pp. 111-134.

7. Jambunathan, K., Lai, E., Moss, M. A., and Button, B. L., 1992, " A Review of Heat Transfer Data for Single Circular Jet Impingement," *Int. J. Heat Fluid Flow*, **13**, pp. 106-115.

8. Ogawa, K., Hijikata, K., 1996, "Experimental and Theoretical Study on Heat Transfer of an Impinging Plasma Jet", HTD-**336/**FED-**240**, *Transport Phenomena in Materials Processing and Manufacturing*, pp. 1-8.

9. Sabirov, I., 2004, "A Numerical Study of a Substrate, Heated by an Impinging Plasma Jet," MS thesis, Department of Mechanical Engineering, Wichita State University.

10. Baughn, J. W., and Shimizu, S., 1989, "Heat Transfer Measurements from a Surface with Uniform Heat Flux and Impinging Jet," *ASME J. Heat Transfer*, **111**, pp. 1096-1098.

11. Lee, D., Greif, R., and Lee, S. J., 1995, "Heat Transfer from a Flat Plate to a Fully Developed Axisymmetric Impinging Jet," *ASME J. Heat Transfer*, **117**, pp. 772-776.

12. Yan, X., Baughn, J. W., and Mesbar, M., 1992, "The Effect of Reynolds Number on the Heat Transfer Distribution from a Flat Plate to an Impinging Jet,"*ASME HTD,* **226**, pp. 1-7.

13. Goldstein, R. J., and Timmer, J. F., 1982, "Visualization of Heat Transfer from Arrays of Impinging Jets," *Int. J. Heat and Mass Transfer*, **25**, pp. 1857-1868.

14. Obot, N.T., Majumdar, A. S., and Douglas, W. J., 1979, "The Effect of Nozzle Geometry on Impingement Heat Transfer Under a Round Turbulent Jet," ASME Paper 79-WA/HT-53.

15. Gordon, R., and Akfirat, J. C., 1965, "The Role of Turbulence in Determining Heat Transfer Characteristics of Impinging Jets," *Int. J. Heat and Mass Transfer*, **8**, pp. 1261-1272.

16. Baukal, C.E., and Gebhart, B., 1995, "A Review of Flame Impingement Heat Transfer Studies Part 2,"*Combustion Science and Tech*., **104**, pp. 359-385.

17. Boguslawski, L., and Popiel, C. O., 1979, "Flow Structure of Free Round Turbulent Jet in the Initial Region," *J. Fluid Mechanics*, **90**, pp. 531-539.

18. Hollworth, B. R., and Wilson, S. I., 1984, "Entrainment Effects on Impingement Heat Transfer: Part I - Measurements of Heated Jet Velocity and Temperature Distributions and Recovery Temperatures on Target Surface," *J. Heat Transfer*, **106**, pp. 797-805.

19. Hollworth, B. R., and Gero, L. R., 1985, "Entrainment Effects on Impingement Heat Transfer: Part II - Local Heat Transfer Measurements," *Transactions of the ASME*, **107**, pp. 910 -917.

20. Hoogendoorn, C. J., 1977, "The Effect of Turbulence on Heat Transfer at a Stagnation Point," *J. Heat and Mass Transfer*, **20**, pp. 1333-1338.

21. Lytle, D., and Webb, B. W., 1982, "Air Jet Impingement Heat Transfer at Low Nozzle-Plate Spacing," *Int. J. Heat and Mass Transfer*, **37**, pp. 1857-1868.

22. Kataoka, K., 1990, "Impingement Heat Transfer Augmentation due to Large Scale Eddies," *Proc. 9th Int. Heat Transfer Conf.,* **1**, Hemisphere, Washigton. DC, pp. 255-273.

23. Boulos, M. I., Fauchais, P., and Pfender, E., *Thermal Plasmas, Fundamental Applications*, Plenum Press, New York, pp. 389-423.

24. Ahmed, I., and Bergman, T. L., 2000, "Three Dimensional Simulation of Thermal Plasma Spraying of Partially Molten Ceramic Agglomerates," *J. of Thermal Spray Technology*, **9(2)**, pp. 214-224.

25. Modest, M.F., 1993, *Radiative Heat Transfer*, Mc Graw Hill, New York.

26. Fluent Inc, Lebanon, NH, USA, 1993 Fluent Version 6.0 Manual.